Interfacial Phenomena of Solvent-Diluted Block Copolymers

Shai Cohen and David Andelman*

Raymond and Beverly Sackler School of Physics and Astronomy, Tel Aviv University, Ramat Aviv, Tel Aviv 69978, Israel

ABSTRACT: A phenomenological mean-field theory is used to investigate the properties of solvent-diluted diblock copolymers (BCP), in which the two BCP components (A and B) form a variety of phases that are diluted by a solvent (S). Using this approach, we model mixtures of diblock copolymers and a solvent and obtained the corresponding critical behavior. In the low solvent limit, we find how the critical point depends on the solvent density. Because of the nonlinear nature of the coupling between the A/B and BCP/solvent concentrations, the A/B modulation induces modulations in the polymer–solvent relative concentration with a double wavenumber. The free boundary separating the polymer-rich phase from the solvent-rich one is studied in two situations. First, we show how the presence of a chemically patterned substrate leads to deformations of the BCP film/solvent interface, creation of terraces in lamellar BCP film and even formation of multidomain droplets as induced by the patterned substrate. Our results are in agreement with previous self-consistent field theory calculations. Second, we compare the surface tension between parallel lamellae coexisting with a solvent phase with that of a perpendicular one, and show that the surface tension has a nonmonotonic dependence on temperature. The anisotropic surface tension can lead to deformation of spherical BCP droplets into lens-shaped ones, together with reorientation of the lamellae inside the droplet during the polymer/solvent phase separation process in agreement with experiment.

I. INTRODUCTION

A wide variety of chemical and physical systems exhibiting patterns and textures can be characterized by spatial modulations in thermodynamical equilibrium. Some of the most common morphologies are stripes and circular droplets in two dimensions (2d), as well as sheets, tubes and spherical droplets in three dimensions (3d). These systems are very diverse and include type I superconductor films, ferromagnetic films, block copolymers (BCP), and even lipid biomembranes.[1–3] In each case, the physical origin of the order parameter and the pattern characteristic differ with length scales or periodicity that vary from mesoscopic scales of tens of nanometers in biological membranes[4] to centimeters in ferrofluids.[2,3] The fact that such a vast variety of physical, chemical, and biological systems display morphological similarities, irrespective of the details of microscopic structure and interactions, is striking and can be explained by a generic mechanism of competing interactions.[1–3]

A Ginzburg–Landau (GL) expansion[5] applicable to modulated phases was introduced[6] by adding to the free energy a term preferring a specific wavelength q_0. This GL-like approach works rather well close to the critical point (weak segregation limit), and its advantage lies in its simplicity and analytical predictions. The added term in the GL free-energy expansion can be written as:

$$\frac{1}{2} \int [(\nabla^2 + q_0^2)\phi]^2 \, \mathrm{d}^2 r \tag{1}$$

This positive-definite form is known as the Brazovskii form,[6–12] and has a minimum at q_0. Close to the critical point (the weak segregation limit), also called the order–disorder temperature

(ODT) in BCP systems, it has been shown by Brazovskii[6] and Leibler[7] that the amplitude of the most dominant q-mode, q_0, grows much faster than other q-modes. This free-energy form and similar ones have been used extensively in the past to calculate phase diagrams and grain boundaries of modulated phases,[13–15] as well as to study the effects of chemically patterned surfaces on such phases.[16–22] In particular, such coarse-grained models compare well with experimental phase diagrams[23] and grain boundaries studies of BCP.[24–26] Other and more accurate numerical schemes exist and rely on self-consistent field theories (SCFT), as well as Monte Carlo simulations. For a recent review of these complementary techniques see, e.g., ref 27.

In the present study, we consider an extension of modulated phases that are diluted by a solvent. Although our phenomenological approach can apply to any modulated phase, we apply it explicitly to symmetric lamellar phases of BCP diluted by a solvent in a variety of solvent conditions.[28] For example, in bad solvent conditions the phase separation between a BCP-rich phase and a solvent-rich phase allows us to explore the free interface between a BCP film and bad solvent (vapor). Our study is relevant to a large number of experimental situations where a BCP film is spin-casted on a solid substrate.[29–39] As the solvent evaporates, the polymer/air free interface can deform, and the free interface self-adjust its shape in order to minimize the total free energy. Another focus of our study is to consider the shape and orientation of
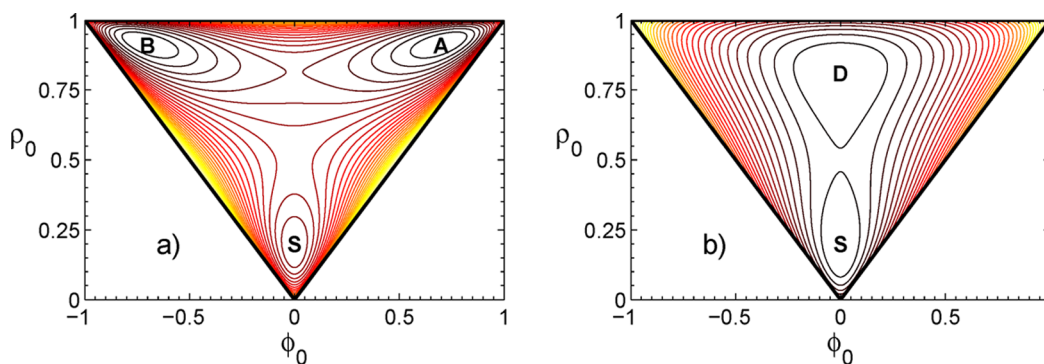
Figure 1. Free-energy landscape in the (ϕ_0, ρ_0) plane. The contour plot is obtained from the ternary-mixture free energy, eq 5, disregarding the spatially varying terms, for $\chi = 4.4$ and $\mu_\rho = \mu_\phi = 0$. In (a) $\tau = 1.45 > \tau_c$ while in (b) $\tau = 0.5 < \tau_c$. In part a, the free-energy minima are denoted by A, B, and S and in part b by D and S.

multilamellar BCP domains, during phase separation between the polymer and a bad solvent.

The outline of our paper is as follows. In the next section we present our model, which is a generalization of phenomenological free-energy expansions used to model pure di-BCP systems. The free energy includes additional terms that depend on the solvent (S) and its coupling with the A/B relative composition. In section III, we present the bulk properties of the solvent-diluted BCP system, including an explanation of the period-doubling phenomena found for the polymer density and an analysis of the critical point in the low-solvent limit. In section IV, we present results for grain boundaries between lamellar domains of different orientations, and show how a chemically patterned substrate influences deformations of a flat free interface and formation of BCP droplets. We then proceed by calculating the temperature dependence of the lamellar-solvent surface tension for parallel and perpendicular lamellar orientations. We also show how such an anisotropic surface tension affects the shape of circular lamellar drops of BCP during the overall solvent/polymer phase separation process and compare with experiments.

II. THE FREE-ENERGY OF MIXING

In this study we employ a phenomenological free-energy of mixing[40,41] of a ternary mixture composed of three components: A, B, and S. The A and B components are the two components of a di-BCP[13] and have volume fractions ϕ_A and ϕ_B, while S is a solvent with volume fraction ϕ_S. All three volume fractions satisfy $0 \leq \phi_i \leq 1$, $i = A, B, S$.

Using the incompressibility condition

$$\phi_A + \phi_B + \phi_S = 1 \qquad (2)$$

it is more convenient to consider the two following order-parameters:

$$\rho = \phi_A + \phi_B,$$
$$\phi = \phi_A - \phi_B \qquad (3)$$

where $0 \leq \rho \leq 1$ is the solute (BCP) volume fraction and $-1 \leq \phi \leq 1$ is the relative A/B concentration of the two blocks, satisfying $|\phi| \leq \rho$.

We work in the grand-canonical ensemble where the Gibbs free-energy density (per unit volume) g is defined as

$$g = \varepsilon - Ts - \sum_{i=A,B,S} \mu_i \phi_i \qquad (4)$$

with T being the temperature, ε the enthalpy, $s = -k_B \sum_i \phi_i \ln(\phi_i)$ the ideal entropy of mixing, and μ_i the chemical potential of the i-th species. Writing ε in terms of all two-body interactions between the three components, and expressing the free-energy g in terms of the ρ and ϕ densities, yields

$$
\begin{aligned}
\frac{g(\phi, \rho)}{k_B T} = & -\frac{\tau}{2}\phi^2 + \frac{\chi}{2}\rho(1-\rho) + v_{\phi\rho}\phi(1-\rho) - \mu_\phi\phi \\
& - \mu_\rho\rho + \frac{\rho+\phi}{2}\ln(\rho+\phi) + \frac{\rho-\phi}{2}\ln(\rho-\phi) \\
& + (1-\rho)\ln(1-\rho) + \frac{H}{2}[(\nabla^2 + q_0^2)\phi]^2 + K(\nabla\rho)^2
\end{aligned}
$$

$$(5)$$

where τ is the interaction parameter between the A and B monomers of the BCP, χ is the solvent−polymer interaction parameter, and $v_{\phi\rho}$ is the parameter denoting any asymmetry in the interaction between the solvent and the A and B components. For simplicity, throughout this paper we set $v_{\phi\rho} = 0$, modeling only symmetric interactions of the A and B components with a neutral S solvent. Clearly that in this case all our results will obey the symmetry $\phi \leftrightarrow -\phi$.

The next two terms are the chemical potential ones, where μ_ϕ couples linearly to ϕ and μ_ρ to the polymer volume fraction ρ, and the three logarithmic terms originate from the ideal entropy of mixing. So far the terms of the free energy, g, describe any three-component mixture of A, B and S within the ideal solution (mean-field) theory. In order to model the A/B mixture as a di-BCP, we add to eq 5 the H-term as introduced in eq 1, where H is the modulation coefficient and q_0 is the most dominant wavevector.[6−11,13,14] As we are interested in studying interfacial phenomena between polymer-rich and solvent-rich phases, we also included a gradient squared term in the polymer density ρ to account for the cost of density fluctuations, where $K > 0$ is a measure of the interface "stiffness".[42]

Note that for the symmetric $v_{\phi\rho} = 0$ case, the only coupling terms in eq 5 between the two order parameters, ϕ and ρ, comes from the entropy, and are even in ϕ. There is no bilinear term $\phi\rho$ and the lowest-order coupling term is $\phi^2\rho$. The free energy can be reduced to two simple limits. (i) For $\rho = 1$, the system reduces to the pure A/B BCP. Here $\phi_S = 0$ and

$$\frac{g}{k_BT} = -\frac{\tau}{2}\phi^2 + \frac{1+\phi}{2}\ln(1+\phi) + \frac{1-\phi}{2}\ln(1-\phi)$$
$$+ \frac{H}{2}[(\nabla^2 + q_0^2)\phi]^2 - \mu_\phi\phi \tag{6}$$

This case was mentioned in section I and has been studied extensively in the past for pure BCP systems.[6,7] The BCP phase has a critical point (ODT) at $\tau_c = 1$ and for $\tau > \tau_c$, only the disordered phase is stable.

(ii) Another simple limit is obtained by setting $\phi_0 = 0$ (or $\phi_A = \phi_B$), yielding

$$\frac{g}{k_BT} = K(\nabla\rho)^2 + \frac{\chi}{2}\rho(1-\rho) + \rho\ln\rho$$
$$+ (1-\rho)\ln(1-\rho) - \mu_\rho\rho \tag{7}$$

This is the free energy of a solvent/solute binary mixture, where ρ is the solute volume fraction.[40] In the bulk, $\rho = const$, and one gets a demixing curve between two macroscopically separated phases. The demixing curve terminates at a critical point located at $\chi_c = 4$ and $\rho_c = 0.5$.

III. BULK PROPERTIES

A. The Low Solvent Limit and Criticality. Since our free energy reduces to eq 6 for $\rho_0 = 1$ (no solvent), a BCP phase for the pure A/B system exists as long as $\tau > \tau_c$, where $\tau_c(\rho_0 = 1) = 1$ is the critical point (ODT). To gain some insight of the behavior for the ternary system with $\rho_0 < 1$, we plot in Figure 1 typical energy landscapes corresponding to the free energy g of eq 5 without the spatial-dependent H and K terms. In Figure 1a, $\tau = 1.45$ is above the critical point, $\tau_c = 1$, and we notice three local minima denoted by A, B and S. The A and B minima denote two equivalent points for which the solute density is high ($\rho_0 \approx 0.9$) and is composed mainly of the A component ($\phi_0 \approx 0.7$) or the B component ($\phi_0 \approx -0.7$). Point S, on the other hand, has low solute density ($\rho_0 \simeq 0.2$) and is composed of an equal amount of the A and B ($\phi_0 = 0$). In addition, note also that the free energy is concave on the $\rho_0 = 1$ line.

Part a of Figure 1 should be compared with part b, for which $\tau = 0.5 < \tau_c = 1$. In this case, only two minima exist and are denoted as S (solvent rich as before) and D (disorder solute-rich). For the D minimum, the concentration ρ_0 is high and equal amounts of A and B component are present ($\phi_0 = 0$). The free energy is convex on the $\rho_0 = 1$ line. We conclude that modulations can only occur if the A and B minima exist so that the two component tend to phase separate, while the modulation term dictates the length scale of spatial modulations by having the ϕ composition oscillates between these two states. Looking at Figure 1a along the symmetric $\phi_0 = 0$ line, we further remark that the free energy changes from being slightly concave at $\rho_0 \lesssim 1$ to highly convex close to $\rho_0 = 0$. This change in convexity suggests that a lamellar phase in ϕ will only be energetically favorable at $\rho_0 \simeq 1$, because in the highly convex region only one minimum exists. It also suggests that the critical point τ_c will grow as ρ_0 decreases below $\rho_0 = 1$.

Next, we would like to obtain an analytical expression of $\tau_c(\rho)$, for $\rho \lesssim 1$, while recalling that without any solvent, $\tau_c(\rho = 1) = 1$. We use the lamellar single-mode approximation, and expand the free energy in powers of ϕ/ρ. Because $|\phi| < \rho$, ϕ/ρ may serve as a small expansion parameter around the ($\rho_0 \simeq 1$, $\phi_0 = 0$) corner of the phase diagram. Expanding the entropy in eq 5 to fourth order in ϕ/ρ results in

$$\frac{g}{k_BT} \simeq -\frac{\tau}{2}\phi^2 + \frac{\chi}{2}\rho(1-\rho) + (1-\rho)\ln(1-\rho)$$
$$+ \rho\ln\rho + \frac{\phi^2}{2\rho} + \frac{\phi^4}{12\rho^3} + \frac{H}{2}[(\nabla^2+q_0^2)\phi]^2 + K(\nabla\rho)^2$$
$$- \mu_\rho\rho - \mu_\phi\phi \tag{8}$$

Since the only source of modulations is the $H/2[(\nabla^2 + q_0^2)\phi]^2$ term, modulations in ρ can be induced by modulations in ϕ through the coupling between ϕ and ρ (that in our model originates only from the entropy terms) as will be explain in detail in section III.B below. Thus, it is reasonable to assume that close to the critical point, where ϕ starts to modulate, the modulations in ρ are small and their effect on the ϕ modulations can be neglected (to be further justified below).

Dropping the constant terms in ρ from eq 8 yields

$$\frac{g}{k_BT} = -\frac{\tau}{2}\phi^2 + \frac{\phi^2}{2\rho} + \frac{\phi^4}{12\rho^3} + \frac{H}{2}[(\nabla^2 + q_0^2)\phi]^2 \tag{9}$$

Assuming for simplicity 1d lamellar modulations that are symmetric around $\phi_0 = 0$, we use for ϕ the single-mode ansatz $\phi(x) = \phi_0 + \phi_q\cos(q_0x)$, where the spatial average of $\phi(x)$ for the symmetric case is $\phi_0 = \langle\phi\rangle = 0$, and ϕ_q is its modulation amplitude, while $\rho(x)$ is taken without any spatial modulations and is equal to its spatial average, $\rho_0 = \langle\rho\rangle$.[43−46] Taking a variation with respect ϕ_q, it can be shown that for the most dominant mode, $q = q_0$, its amplitude ϕ_q satisfies:

$$\phi_q^2 = 4\rho_0^3\left(\tau - \frac{1}{\rho_0}\right) \tag{10}$$

From eq 10, we get a condition for the extent of the lamellar phase by requiring that $\phi_q^2 \geq 0$, and the critical temperature is obtained at $\phi_q = 0$:

$$\tau_c = 1/\rho_0 \tag{11}$$

The above equation agrees with $\tau_c = 1$ for $\rho_0 = 1$. Furthermore, for $\rho_0 \to 0$ we get $\tau_c \to \infty$, implying that the only possible phase at low solute concentrations is the disordered phase.

B. Induced Period Doubling in ρ. The modulations in ϕ cause the overall BCP density, ρ, to modulate as well. Interestingly, the modulations in ρ are found to have half the wavelength of the ϕ modulations. We would like to explain how this period doubling phenomenon is manifested in our formalism, and note that it has been already suggested and is not unique only to the lamellar phase.[47,48]

In Figure 2, such oscillations in ϕ and ρ can be clearly seen, where the amplitude of the ρ oscillations is much smaller than the ϕ ones. The reason for such oscillations is the nonlinear coupling between the ϕ and ρ order parameters. As we restrict ourselves to the case of symmetric interactions between A/S and B/S, $v_{\phi\rho} = 0$ in eq 5; thus, this coupling originates in our model only from the entropy terms. Note that in Figure 2 and in all subsequent figures we have chosen for convenience $H = K = 1$ and $q_0 = 1/\sqrt{2}$.

In Figure 3 we show the contour plot of the free energy for $\chi = 4.2$ and $\tau = 1.45$. The spatial modulations in ϕ can be represented as an oscillatory path between the two free-energy minima denoted as A and B. The path between the two points will not take the direct route denoted by "1" for which $\rho = const$, but rather a curved and longer route denoted by "2",

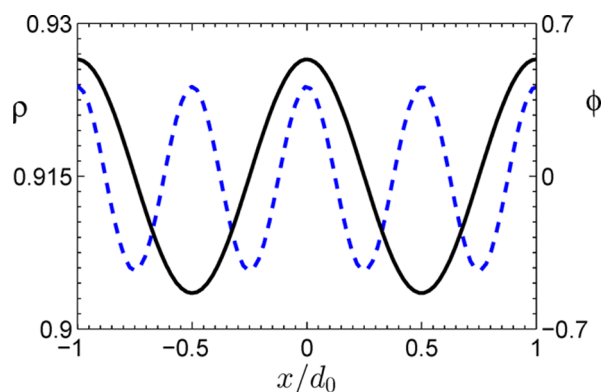**Figure 2.** Spatial modulation of ρ (dashed line) and ϕ (solid line) are plotted as a function of x/d_0, with $d_0 = 2\pi/q_0$. The parameter values: $\tau = 1.2$, $\chi = 5.5$, $\mu_\phi = 0$ and $\mu_\rho = 0$ result in $\langle\rho\rangle = 0.915$ and $\langle\phi\rangle = 0$. The oscillations in ρ have half the wavelength of the ϕ ones. The length scale of the ρ modulations ($\rho_q = 0.0091$) is much smaller than the ϕ ones ($\phi_q = 0.538$). The other parameter values are $H = K = 1$ and $q_0 = 1/\sqrt{2}$.
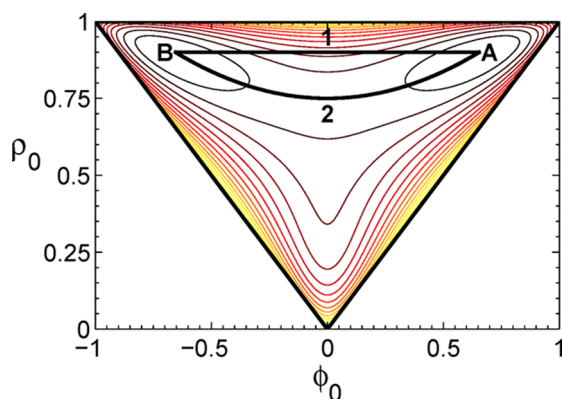

Figure 3. Two possible routes from point A to B, plotted on the free-energy contour plot in the (ϕ_0, ρ_0) plane, with $\chi = 4.2$, $\tau = 1.45$, $\mu_\rho = 0.05$ and $\mu_\phi = 0$. "1" is a straight route in which ρ does not change, while "2" is a curved one. The curved "2" path is energetically preferred as it bypasses the energy barrier along the direct "1" path between A and B.

because the latter is energetically preferred as it avoids the energy barrier along the direct path. Thus, oscillations in the ϕ order parameter induce oscillations in ρ. The fact that the ρ wavenumber is doubled ($2q_0$), as compared with the ϕ wavenumber (q_0), can also be understood from Figure 3. For each cycle going from A to B and back, ϕ completes one cycle, while ρ completes two cycles. We note that increasing χ will cause these oscillations to decrease their magnitude as the potential well in the ρ direction moves to higher values of ρ and becomes deeper.

We calculate the induced ρ modulations along one spatial direction, taken to be the x-direction; namely, $\rho = \rho(x)$ and $\phi = \phi(x)$. An analytical (yet approximate) expression of the modulation amplitudes can be obtained by expanding the free energy, eq 8, in powers of $\eta(x) = \rho(x) - \rho_D$ around the value of the disordered phase, ρ_D, to second order in ρ. Because the oscillations in ϕ are between two local minima, we can further expand eq 8 to fourth order in ϕ:

$$\frac{g}{k_B T} \simeq -\frac{\tau}{2}\phi^2 + \frac{\phi^2}{2\rho_D} + \frac{\phi^4}{12\rho_D{}^3} - \frac{\phi^2}{2\rho_D{}^2}\eta$$
$$+ \frac{1}{2}\left[\frac{1}{\rho_D} + \frac{1}{1-\rho_D} - \chi + \frac{\phi^2}{2\rho_D{}^3}\right]\eta^2 + K(\eta')^2$$
$$+ \frac{H}{2}[\phi'' + q_0^2\phi]^2 \tag{12}$$

where constant terms are omitted and ρ_D is given by

$$\frac{\chi}{2}(1 - 2\rho_D) + \ln\rho_D - \ln(1-\rho_D) - \mu_\rho = 0. \tag{13}$$

Taking the variation of g in eq 12 with respect to η and using the lamellar single-mode approximation, $\phi = \phi_q\cos(q_0 x)$ for symmetric lamellae, $\langle\phi\rangle = 0$, the inhomogeneous differential equation for $\eta(x) = \rho(x) - \rho_D$ is:

$$2K\eta'' - \frac{1}{2}\left[\frac{1}{\rho_D} + \frac{1}{1-\rho_D} - \chi + \frac{\phi_q^2}{2\rho_D{}^3} + \frac{\phi_q^2}{2\rho_D{}^3}\cos(2q_0 x)\right]\eta$$
$$= -\frac{\phi_q^2}{4\rho_D{}^2}[1 + \cos(2q_0 x)] \tag{14}$$

where the linear term in η originates from the quadratic term in the free energy. This term has to be positive because we have made an expansion around the free-energy minimum. It means that the homogeneous solution of $\eta(x)$ is a decaying function and is of no physical interest, since we are only looking for periodic solutions of the bulk phases. The inhomogeneous solution $\eta(x)$, however, is caused by oscillatory cosine terms [RHS of eq 14]. To obtain an approximate solution we take $\rho_D \simeq 1$ and ϕ_q to be small, allowing us to neglect the sum of the two terms, $\phi_q^2(2\rho_D^3)^{-1} + \phi_q^2(2\rho_D^3)^{-1}\cos(2q_0 x)$, as compared with $(1 - \rho_D)^{-1}$. Then, eq 14 simplifies to:

$$2K\eta'' - \frac{1}{2}\left[\frac{1}{\rho_D} + \frac{1}{1-\rho_D} - \chi\right]\eta$$
$$= -\frac{\phi_q^2}{4\rho_D{}^2}\cos(2q_0 x) - \frac{\phi_q^2}{4\rho_D{}^2} \tag{15}$$

Hence, the inhomogeneous solution has the form $\eta = \eta_0 + \eta_{2q}\cos(2q_0 x)$, with[49]

$$\eta_0 = \frac{\phi_q^2}{4\rho_D{}^2\varepsilon}$$

$$\eta_{2q} = \frac{\phi_q^2}{4\rho_D{}^2(8Kq_0{}^2 + \varepsilon)} \tag{16}$$

where $\varepsilon = \rho_D{}^{-1} + (1-\rho_D)^{-1} - \chi$. This solution represents the period doubling within our model. It makes sense as the modulations in ρ exist only when $\phi_q \neq 0$, and may appear at any value of ρ_D. Larger densities or larger K values (high cost of the polymer/solvent interface) will make the modulations smaller. The fact that $\eta_0 = \langle\eta\rangle \neq 0$ means that a lamellar modulating phase will cause an increase in the average solute density from the disorder phase value, ρ_D.

Comparison between the amplitude η_{2q} as a function of ρ_D as obtained by solving numerically eq 5, and the approximated

analytical one [using eqs 10, 13, and 16] is shown in Figure 4 for various τ values, where symmetric lamellae with $\langle\phi_0\rangle = 0$ are
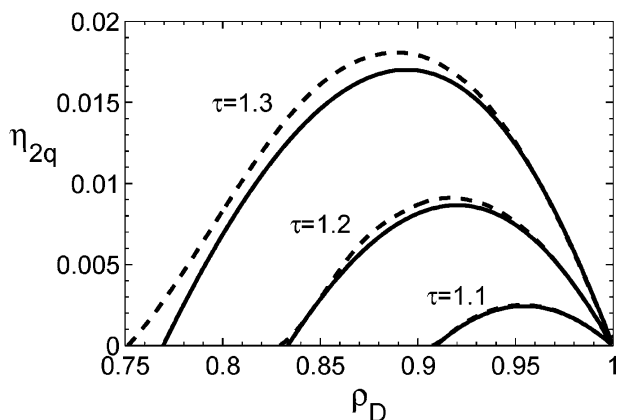

Figure 4. Plot of η_{2q} for symmetric lamellae as a function of ρ_D for three values of $\tau = 1.1, 1.2, 1.3$, and with $\mu_\rho = \mu_\phi = 0$. The dashed line is the numerical solution of eq 5 and the solid line is the analytical approximation of eq 16.

used. At small τ, the accuracy is very good since ϕ_q/ρ_D is small. However, as τ grows so does ϕ_q, and the quality of the approximation deteriorates. Not surprisingly, as $\rho_D \rightarrow 1$, the modulations in ρ disappear. For large τ, the approximation worsens not only when ϕ_q becomes large, but also next to the critical density $\rho_c = 1/\tau$ when ρ_D becomes smaller.

IV. INTERFACES AND BOUNDARIES

A. Grain Boundaries of Solvent-Diluted Lamellae. We proceed by obtaining grain boundaries separating lamellar domains of different orientations. This problem was considered in the past for pure BCP boundaries,[13,15] and here we extend it to solvent-diluted BCP lamellae. The lamellar/lamellar grain boundaries are obtained by minimizing numerically the free energy in a simulation box, with boundary conditions that are periodic on the vertical walls, while the top and bottom surfaces of the simulation box induce lamellar order with different orientations. Such 2d patterns in ϕ and ρ can be seen in Figures 5 and 6. The left panels show the ϕ patterns, whereas the right
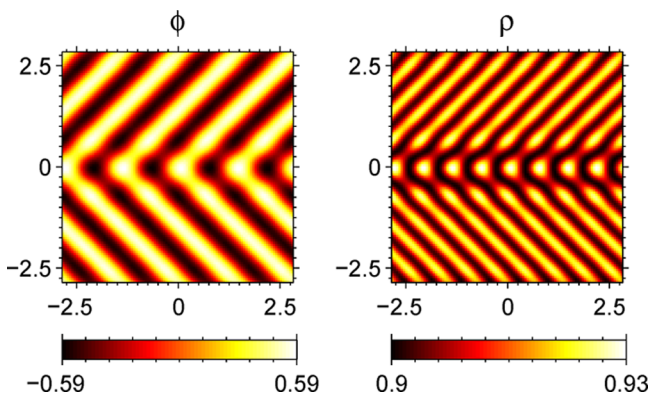

Figure 5. Omega-shaped grain boundary, also called "chevron", between two lamellar grains that meet each other with a fixed angle. The angle is preset to be 90 degrees, and the parameter values are $\tau = 1.2$, $\mu_\rho = -0.004236$, $\chi = 5.5$ and $\mu_\phi = 0$. The axes are given in units of $d_0 = 2\pi/q_0$, and the color bar accounts for variation of the ϕ (left) and ρ (right) order parameters.
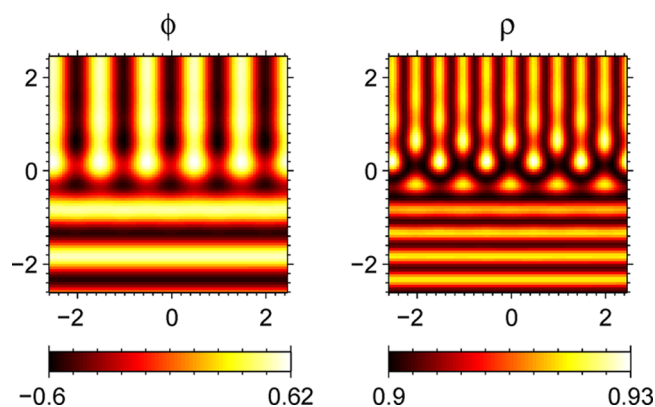

Figure 6. T-junction grain boundary between two perpendicular lamellar domains. The parameter values are $\tau = 1.2$, $\chi = 5.5$, $\mu_\rho = -0.004236$, and $\mu_\phi = 0$. The axes are given in units of $d_0 = 2\pi/q_0$, and the color bar accounts for variation of the ϕ (left) and ρ (right) order parameters.

panels show the corresponding ρ ones with a doubled wavenumber in their spatial periodicity, as was discussed in section III.B.

Omega-shaped tilt grain boundaries (Figure 5) and T-junction grain boundaries (Figure 6) are shown as examples of possible grain boundaries between lamellar phases and agree well with previous works on pure BCP systems.[13,15] Because of the wavenumber doubling effect one can see in both figures "bulbs" of higher density at the grain boundaries, which is more pronounced for the ρ patterns than for the ϕ ones. This result is in agreement with experiments on dilute BCP systems[50] and calculations on blends of BCP and homopolymer acting as a solvent, which show that the homopolymer density is higher at the interfaces (e.g., T-junction). This probably can be explained in terms of a mechanism where the solvent molecules accumulate at the location where the BCP chains have large deformation and, hence, release some of their strain at the interface.[50]

In general, the solvent is enriched at the interface in order to dilute the unfavorable interactions between the two polymer species. Since a BCP lamella contains two A/B interfaces, their distance is half the lamellar spacing and can be obtained in other types of grain boundaries, as well as at interfaces between two coexisting phases at equilibrium.[47,48]

B. Substrate Chemical Patterning. Chemically and topographically patterned surfaces with preferential local wetting properties toward one of the two polymer blocks result in a unique organization of BCP thin films and have been investigated thoroughly in experiments.[32−39] We will explore here the interplay between such chemical heterogeneities on surfaces and the structure of BCP thin films.

The bulk BCP phase is placed in contact with a chemically patterned surface, modeled by two surface interactions: σ_ρ and σ_ϕ,[11,20] which are coupled linearly to ρ and ϕ, respectively. They lead to a new surface term G_s in the free energy

$$G_s = k_B T \int d^2\mathbf{r}_s \left[\sigma_\rho(\mathbf{r}_s)\rho(\mathbf{r}_s) + \sigma_\phi(\mathbf{r}_s)\phi(\mathbf{r}_s)\right] \quad (17)$$

where $\mathbf{r}_s$ is a vector on the 2d substrate. As an illustration of the chemical pattern influence on a BCP lamellar phase, we examine the effect of the patterned substrate on structure and orientation of a parallel ($L_\parallel$) lamellar phase as can be seen in Figure 7. The substrate is constructed in such a way that its

field, σ_ϕ, prefers the B component in the surface midsection, while is neutral elsewhere:

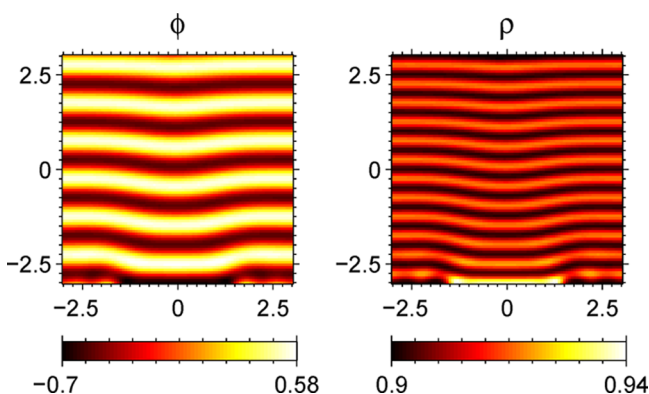$$\sigma_\phi = \begin{cases} 0.5, & |x| \leq 1.5d_0 \\ 0, & |x| > 1.5d_0 \end{cases} \tag{18}$$

Figure 7. ϕ (left) and ρ (right) order parameters for a symmetric bulk lamellar phase, $\phi_0 = 0$, for a substrate that prefers the B component in its central section as in eq 18, while we set periodic boundary conditions on the side walls. The axes are given in units of $d_0 = 2\pi/q_0$, and the color bar accounts for variation of each order parameter. The patterns are produced using eq 5 with $\chi = 5.5$, $\tau = 1.2$ $\mu_\rho = -0.004236$, $\mu_\phi = 0$, for which the lamellar phase is the equilibrium phase.

In addition, the field σ_ρ is fixed to be zero on the entire substrate. The upper bounding surface of the simulation box is taken as neutral, while the vertical walls obey periodic boundary conditions. The deformation of the lamellar structure due to the surface pattern are clearly seen close to the substrate and decays fast into the lamellar bulk as was previously studied for pure BCP systems.[11]

C. The Free Interface. We can also address within our model and numerical scheme the *free interface* between a thin lamellar film in coexistence with a bad solvent (vapor),[28,51] as is schematically plotted in Figure 8. In particular, and motivated by experimental set-ups, we explore deformations of such a free interface and their coupling with domain nucleations as induced by different surface chemical patterings.

In order to allow deformations of the free interface, we consider specifically the case where the segregation in ρ is weak but that of ϕ is still strong. This is done by choosing $\tau = 1.8$, χ
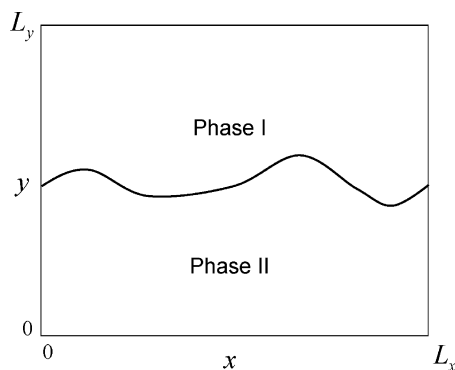

Figure 8. Schematic drawing of an interface separating two coexisting phases, denoted as "Phase I" and "Phase II". The 2d system volume is $V = L_x \times L_y$ and the interface projected area is $A = L_x$.

$= 4.1$, and $\mu_\rho = -0.101682$ (and $\mu_\phi = 0$ for symmetric lamellae), while recalling that the critical point values are $\tau_c = 1$ and $\chi_c = 4$ (see section II). The effect of surface-induced modulation on a weakly segregated interface is seen in Figure 9,
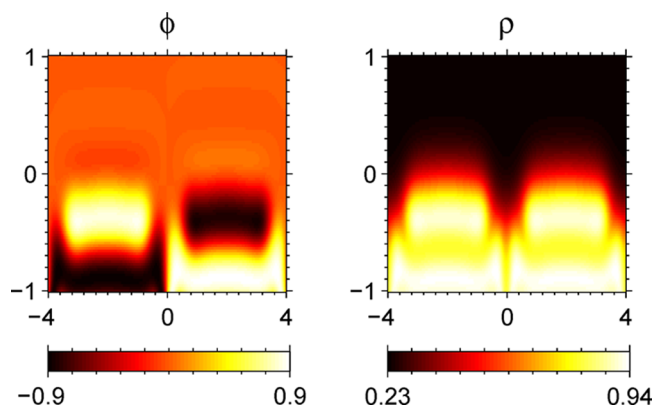

Figure 9. Terrace formation both in ϕ (left) and ρ (right) for a lamellar structure due to patterned substrate as in eq 19. The system is at its solvent-lamellar coexistence with $\tau = 1.8$, $\chi = 4.1$, $\mu_\rho = -0.101682$ and $\mu_\phi = 0$. The axes are given in units of $d_0 = 2\pi/q_0$, and the color bar accounts for variation of each order parameter.

where the lower surface is chosen to have the following step pattern:

$$\sigma_\phi = \begin{cases} -0.1, & 0 \leq x < 4d_0 \\ 0.1, & -4d_0 \leq x < 0 \end{cases} \tag{19}$$

and $\sigma_\rho = 0$ for the entire substrate. This patterning causes a defect formation at the midpoint $x = 0$, where the change in σ_ϕ occurs. The defect, in turn, induces a deformation of the solvent/polymer (free) interface, forming several terraces. The jumps in terrace height is about half of the lamellar periodicity, in agreement with previous results obtained on free interfaces in contact with chemical patterns using self-consistent field theory (SCFT).[28]

A defect can also be obtained between the two lamellar orientations: parallel to the substrate ($L_\parallel$) and perpendicular one ($L_\perp$) by choosing a patterned substrate that prefers the $L_\parallel$ one in its midsection and an $L_\perp$ elsewhere:

$$\sigma_\phi = \begin{cases} 0.1, & |x| \leq 2d_0 \\ 0, & 4d_0 > |x| > 2d_0 \end{cases} \tag{20}$$

and $\sigma_\rho = 0$ for the entire substrate. As can be seen in Figure 10, this surface pattern causes a deformation of the free interface between the BCP (lamellar) and solvent phases. In the midsection, $L_\parallel$ has a thickness of three layers ($y \approx 1.5d_0$), and a terrace then separates the midsection $L_\parallel$ from the side ones where the $L_\perp$ is the preferred orientation. Moreover, the $L_\perp$ phase is deformed and tilted at the boundary with the $L_\parallel$ phase, and the width of this boundary increases as τ approaches its critical value.

Another way of deforming the free interface is to induce a BCP droplet by a patterned substrate in coexistence with the solvent phase. For that purpose the substrate is separated into a central section that prefers the BCP with $\sigma_\rho < 0$ (BCP wetting condition), while on the rest of the surface $\sigma_\rho > 0$, which repels the lamellar phase (nonwetting condition that prefers the solvent). In addition, by manipulation the σ_ϕ field, we can
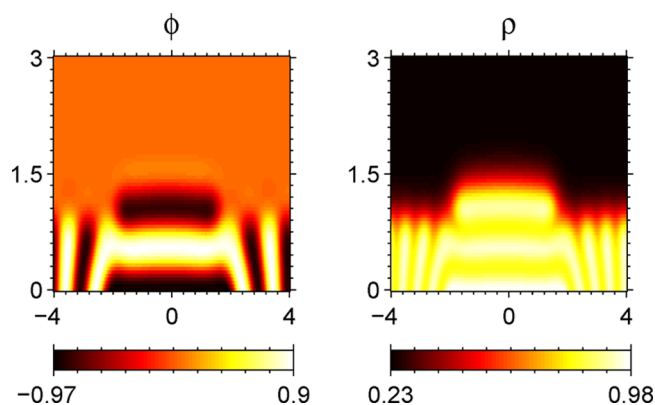
Figure 10. Parallel ($L_∥$) and perpendicular ($L_⊥$) domains in equilibrium with a pure solvent phase ($\sigma_\rho = 0$) in presence of a surface pattern as in eq 20. Terrace formation and deformation of the free (solvent/BCP film) interface can be seen. The system parameters are: $\tau = 1.8$, $\chi = 4.1$, $\mu_\rho = -0.101682$, and $\mu_\phi = 0$. The axes are given in units of $d_0 = 2\pi/q_0$, and the color bar accounts for variation of the ϕ (left) and ρ (right) order parameters.

induce different domains inside the same droplet. Such a case in which both $L_⊥$ and $L_∥$ domains coexist within the same BCP droplet is shown in Figure 11, with σ_ρ and σ_ϕ given by:

$$\sigma_\rho = \begin{cases} -0.5, & |x| \leq 5d_0 \\ 0.5, & 6d_0 > |x| > 5d_0 \end{cases}$$

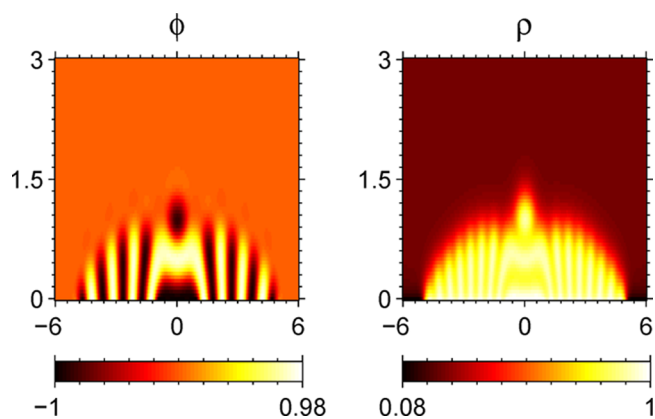$$\sigma_\phi = \begin{cases} 0.5, & |x| \leq d_0 \\ 0, & 6d_0 > |x| > d_0 \end{cases} \tag{21}$$

Figure 11. BCP lamellar droplet wetting a substrate. The ϕ (left) and ρ (right) order parameters are plotted. The wetting is formed using a surface field that attracts the BCP to its midsection and repels it elsewhere, as in eq 21. Domains of different orientations are further induced inside the lamellar droplet by a σ_ϕ surface field [eq 21]. The lamellar/solvent phase coexistence occurs for $\tau = 1.8$, $\chi = 4.1$, $\mu_\phi = 0$, and $\mu_\rho = -0.101682$. The axes are given in units of $d_0 = 2\pi/q_0$, and the color bar accounts for variation of each order parameter.

The patterning leads to central domain of the droplet in the $L_∥$ orientation surrounded by two deformed $L_⊥$ domains that compensate between the height of the $L_∥$ phase and the edges of the droplet. The morphologies and free-interface profiles found in this section result from substrate patterning, and are in agreement with the ones obtained recently using a more computationally intensive method of SCFT.[28]

D. Surface Tension of Lamellar Phases. As seen in the preceding sections, our model describes different types of coexisting phases and their interfaces. We proceed by analyzing the surface tension between a solute-rich lamellar phase and a solvent-rich disordered phase as a function of the phase separation controlling parameters: τ and χ. An illustration of the two coexisting phases in shown schematically in Figure 8, and our calculations are performed for $2d$ systems of volume $V = L_x \times L_y$. The surface tension between any two coexisting phases (I and II), is defined as $\gamma = [G^{I,II}(V, A) - V/2(g_b^I + g_b^{II})]/A$, where $A = L_x$ is the projected area of the interfacial layer, and for convenience, each of the two phases occupies half of the total volume.

Coexistence between the two phases is achieved by tuning the appropriate chemical potentials. The free energy G^I of a lamellar BCP phase of volume $V/2$ is calculated numerically by imposing periodic boundary conditions on the side boundaries and free boundary conditions on the upper and lower surfaces. The distance between top and bottom surfaces of the box, L_y, is adjusted so that the free energy G^I is minimized. This occurs when L_y is an integer multiple of the modulated periodicity. Therefore, G^I corresponds to a lamellar phase with no defects, and with a free energy density $g_b^I = G^I/(V/2)$. The same (but much simpler) procedure is used to calculate the bulk free energy of the second (disordered) phase, $g_b^{II} = G^{II}/(V/2)$. This procedure is repeated iteratively until we find the chemical potential yielding two coexisting phases with $g_b^I = g_b^{II}$. When the simulation box V is big enough and for the proper chemical potentials, an initial guess of the upper (I) and lower (II) phases will converge into two coexisting phases with a interface in between them.

We would like to compare the surface tension between a symmetric lamellar phase ($\phi_0 = 0$) and a solvent phase where the lamellae meet the L−S interface at different angles, for $\tau > \tau_c$. By choosing proper initial conditions we consider two limiting lamellar orientations: parallel to the interface ($L_∥$) and perpendicular one ($L_⊥$). In principle, other angles θ can be chosen as was done in ref 13 but we only consider the two extreme cases of $\theta = 0$ and $\theta = 90°$. The corresponding surface tensions, $\gamma_∥$ and $\gamma_⊥$, are then computed as a function of τ for $\chi = 4.5$ and plotted on Figure 12. As τ increases above τ_c, the segregation between the A/B components becomes stronger, causing an increases in the density change across the S−L interface. This leads to an increase of the two surface tensions, $\gamma_∥$ and $\gamma_⊥$, to increase.

It is worth noticing that $\gamma_⊥$ is a monotonically increasing function of τ while $\gamma_∥$ is nonmonotonic. However, while the segregation between the A and B component grows, the modulation amplitude reaches saturation, $\phi_q \to 1$, causing the width of the boundary between A and B to diminish. This is in accord with ref 13 where similar trends with τ have been reported at the lamellar-disorder interface (without a solvent).

Comparing the two orientations of the lamellar phase, it is seen that for low values of τ, the transverse orientation is preferred at the interface, while for larger τ values, $L_∥$ is the preferred one. The crossover occurs at $\tau^* \simeq 1.848$ and indicates that the mere existence of the solvent interface may induce a preferred direction of bulk modulations. This result implies that by incorporating steric repulsion (in which $\phi = \rho = 0$ on any of the confining surfaces), the $L_∥$ phase is preferred next to any neutral surface for large τ values.

E. Shapes of Lamellar Droplets: Theory and Experiments. Because $\gamma_⊥$ and $\gamma_∥$ have very different dependence on τ,
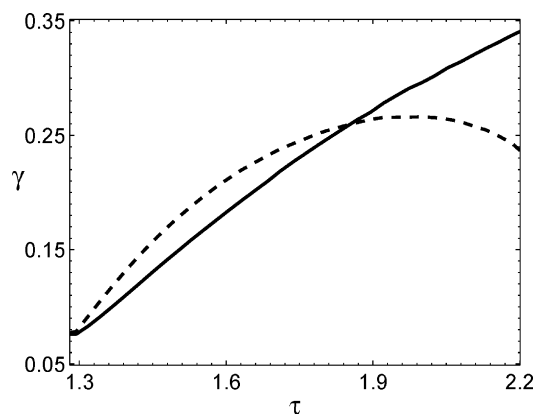
Figure 12. Surface tensions, $\gamma_{\parallel}$ and $\gamma_{\perp}$, for the lamellar–solvent interface for two lamellar orientations, parallel ($L_{\parallel}$, dashed line) and perpendicular ($L_{\perp}$, solid line), as a function of reduced temperature, τ, and for fixed $\chi = 4.5$. The lamellar phase exists only inside the interval $\tau > \tau_c \simeq 1.29$. Up to a crossover $\tau^* \simeq 1.848$, $\gamma_{\perp}$ (solid line) has a lower value than $\gamma_{\parallel}$ (dashed line), and the perpendicular lamellae are preferred. While for $\tau > \tau^*$, $\gamma_{\perp} > \gamma_{\parallel}$ and $L_{\parallel}$ is preferred.

one might expect to see that an initial round droplet containing a lamellar BCP becomes oval. For example, by choosing $\tau = 1.6 < \tau^*$ and $\chi = 4.5$ $\gamma_{\perp} < \gamma_{\parallel}$ causes the $L_{\parallel}$–S interface to reduce its length, while the $L_{\perp} - S$ compensates and increases its length. This is seen in Figure 13. At initial times of the simulation (Figure 13a), we have chosen a circular BCP droplet embedded in a solvent phase. The droplet is circular and the lamellae are preset to orient vertically. At progressive time steps of the simulation, the lamellar orientation deforms so that the lamellae meet the interface at a right angle. As in our simulations the BCP droplet is metastable, it diminishes in size but not in a uniform way. Because the parallel boundary diminishes faster ($\gamma_{\perp} < \gamma_{\parallel}$), the droplet undergoes a continuous shape change, giving the droplet a biconvex lentil-shape at later time steps (Figure 13d). If we continue the simulations even further, the droplet will eventually disappear, since the solvent phase is preferred.

We would like to compare our findings with experimental ones. Formation of lens-like BCP macro-domains embedded in a solvent matrix during solvent/polymer phase separation was observed experimentally[52] for blends of poly(styrene-block-isoprene) and homopolystyrene acting as a bad solvent. The relationship between the macro-phase separation (solvent/BCP) and the self-assembly of the BCP inside the domains was

reported and analyzed. Although we cannot offer a direct explanation of these experiments because our model is restricted to study lamellae in 2d, while in ref 52 cylindrical phases of BCP are studied in 3d, the resemblance of our Figure 13 with Figure 5 of ref 52 is striking, and may be regarded as 2d cuts through the 3d cylindrical BCP domain. We note that in ref 52 a similar explanation for the creation of lens-like domains with orientation of the cylinders along the smaller lens axis was given, and is consistent with a difference in surface tension between the two orientations, $\gamma_{\perp} < \gamma_{\parallel}$.

More recently, addition of Au-based surfactant nanoparticles led to change in shape and morphology for particles based on poly(styrene-b-2-vinylpyridine) diblock copolymers.[53] The added nanoparticles are adsorbed at the interface between block copolymer-containing droplets and the surrounding amphiphilic surfactant. In turn, it causes a preferred perpendicular orientation of the BCP lamellae and led to distortion of the BCP droplets into ellipsoid-shaped ones. The system is more complex as it includes an additional component, but the explanation presented by the authors for the distorted shape is similar to ours and relies on the anisotropic surface tension as enhanced by the added Au nanoparticles.

In another study,[54] lamellar domain formation has been reported following a temperature quench from a disordered BCP phase to the lamellar one. The formed lamellar domains are lens-shaped with their axes along the smaller domain axis. It might be of interest to see if a large change in the final temperature of quenching may cause the formation of lens domains with parallel-oriented lamellae, as is predicted by our study, where $\gamma_{\perp}$ and $\gamma_{\parallel}$ have different (and nonmonotonous) temperature dependence. We also note that the nucleation of a droplet of stable cylinder phase from a metastable lamellar phase was examined within the single-mode approximation for BCP melts in ref 55.

V. CONCLUSIONS

In this paper, we investigate bulk properties of solvent-diluted BCP phases, and a variety of interfaces between coexisting BCP and solvent phases, restricting ourselves to phases with the 1d (symmetric lamellar) morphology. The main assumption made is the dominant nature of a single q_0 mode close to the ODT, which allows us to write a simplified mean-field form of the free energy. Although the dominant q_0-mode can be justified in the weak-segregation limit (close to ODT), we believe that many of the reported results are qualitatively correct also at stronger segregation.
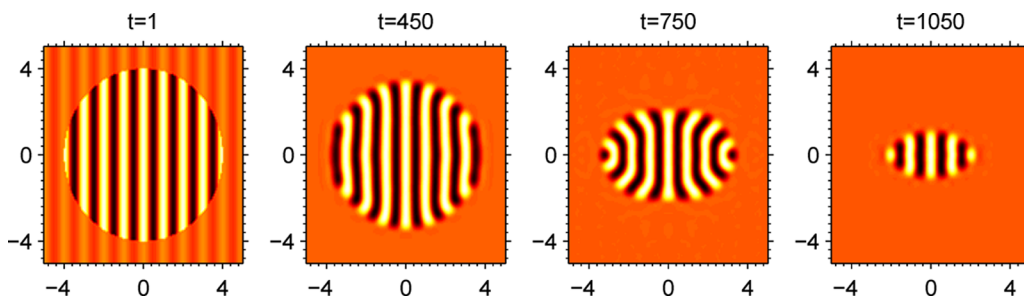

Figure 13. Temporal evolution of the ϕ order parameter of a lamellar BCP droplet in coexistence with a solvent phase. From left to right: $t = 1$, 450, 750 and 1050, where the time step t measures the number of numerical iterations. The parameters used are $\tau = 1.6$, $\chi = 4.5$, $\mu_\rho = -0.058629$, and $\mu_\phi = 0$. As the BCP droplet is metastable, its volume diminishes. The surface tension is anisotropic because the lamellae meet the droplet interface with different angles. It causes the original circular droplet to deform into a biconvex lens-shape, which is preferred energetically. The axes are given in units of $d_0 = 2\pi/q_0$.

To further simplify the model, the numerical investigations are conducted for the case where the interactions between the A and B monomers of the BCP and the solvent (S) are identical. Namely, there is be no bilinear enthalpic term as $\phi\rho$ in the free energy ($v_{\phi\rho} = 0$) of eq 5. Hence, the coupling between the two order parameters, ϕ and ρ, originates only from entropy of mixing that enhances solvent mediation between the two incompatible species. This term is even in ϕ and its leading order is $\phi^2\rho$.

The coupling between ρ, the volume fraction of the solute, and ϕ, the BCP relative A/B composition leads to two interesting analytical results valid in the low solvent limit, $\rho \approx 1$. First, the critical point τ_c that determines the onset of BCP phases becomes ρ dependent, $\tau_c = 1/\rho$. Second, due to the nonlinear nature of the coupling, modulations in ϕ induce modulations in ρ, with a doubled wavenumber, as was explained in detail in section III.B. This phenomenon also results in formation of density bulbs at the interface between a modulated BCP and a disordered phase (Figures 5 and 6).

We show how the presence of a chemically patterned substrate leads to deformations of the free interface separating polymer-rich phase from a solvent-rich one. The patterns can induce formation of terraces in lamellar BCP film and even formation of multidomain droplets. Our results are in agreement with previous self-consistent field theory calculations.[28]

It is of interest to remark on the rotational-symmetry breaking of BCP domains at the BCP/solvent coexistence. We found that the surface tension of the parallel phase ($\gamma_\parallel$) is higher than that of the transverse phase ($\gamma_\perp$) for values of τ close to τ_c, while the opposite occurs for large τ values in agreement with ref 13. This crossover causes a BCP lamellar phase to change its orientation relative to the interface as one changes τ, and should be taken into consideration, as it may be used to induce some preferred direction or interfere with such an attempt. This difference in surface tension causes BCP droplets to deform. We believe that it represents a general phenomenon that can be applied to other situations, such as the shape of domains composed of a hexagonal BCP phase coexisting with a solvent phase.

■ APPENDIX A: NUMERICAL PROCEDURE

The conjugate gradient (CG) method is a well-known numerical algorithm designed to find a local minimum of a smooth, multidimensional nonlinear function.[56] In our case it was applied to minimize the Ginzburg–Landau free-energy expansion, given in eq 5. The main reason for using the CG method is in its convergence efficiency. For a parabolic minimization of a function that depends on N variables, the number of iterations can be reduced from N^2 to about linear in N.

We used a discrete $L_x \times L_y$ simulation box where the order parameters ϕ and ρ depend on the discrete 2d lattice points (x_i, y_j). The total energy is calculated as a sum over all sites, where the differences between the order parameter in one site and its neighboring sites is used to estimate the partial derivatives using their discrete form while penalty functions are used to avoid nonphysical values of the order parameters.

Two types of boundary conditions are used in the numerical procedure. The first are periodic boundary conditions used to simulate bulk behavior. In the second case, the free energy is coupled to some surface field that can be uniform or represents a surface pattern.

As our model does not include random fluctuations, the initial guess of the order parameters, ϕ and ρ, plays an important role. In some cases a random initial guess is used to make the solver converge to the absolute minimum (which is very time demanding), while in other cases a well chosen initial guess is used to speed convergence, especially when it is applied to model the interface between two coexisting phases. We repeated the numerics by starting from several initial conditions in order to check that the convergence is toward the global free-energy minimum.

When the thermodynamics dictates that only one phase is at thermodynamical equilibrium, the average value of the order parameters can be adjusted by changing the chemical potential related to them. In a coexistence region of two (or more) phases defined by setting the chemical potentials to their proper values, the total BCP amount is not conserved for two-phase coexisting phases during the numerical iterations of the CG algorithm. However, the local convergence of the lamellar phase and corresponding interface is much faster and our results indicate qualitatively the system state.

■ AUTHOR INFORMATION

Corresponding Author

*E-mail: (D.A.) andelman@post.tau.ac.il.

Notes

The authors declare no competing financial interest.

■ REFERENCES

(1) Seul, M.; Andelman, D. *Science* **1995**, *267*, 476.
(2) Andelman, D.; Rosensweig, R. E. In *Polymers, Liquids and Colloids in Electric Fields: Interfacial Instabilities, Orientation, and Phase-Transitions*; Tsori, Y., Steiner, U., Ed.; Series in Soft Condensed Matter; World Scientific: Singapore, 2009; Vol. 2, Chapter 1, pp 1–56.
(3) Andelman, D.; Rosensweig, R. E. *J. Phys. Chem. B* **2009**, *113*, 3785.
(4) Leibler, S.; Andelman, D. *J. Phys. (Fr.)* **1987**, *48*, 2013.
(5) Plischke, M.; and Bergersen, B., *Equilibrium Statistical Physics*; World Scientific: Singapore, 2006.
(6) Brazovskii, S. A. *Sov. Phys. JETP* **1975**, *41*, 85.
(7) Leibler, L. *Macromolecules* **1980**, *13*, 1602.
(8) Fredrikson, G. H.; Helfand, E. *J. Chem. Phys.* **1987**, *87*, 697.
(9) Fredrickson, G. H.; Binder, K. *J. Chem. Phys.* **1989**, *91*, 7265.
(10) Hamley, I. W.; Podneks, V. E. *Macromolecules* **1997**, *30*, 3701.
(11) Tsori, Y.; Andelman, D. *Macromolecules* **2001**, *34*, 2719.
(12) Thiele, U.; Archer, A. J.; Robbins, M. J. *Phys. Rev. E* **2013**, *87*, 042915.
(13) Netz, R. R.; Andelman, D.; Schick, M. *Phys. Rev. Lett.* **1997**, *79*, 1058.
(14) Andelman, D.; Brochard, F.; Joanny, J. F. *J. Chem. Phys.* **1987**, *86*, 3673.
(15) Tsori, Y.; Andelman, D.; Schick, M. *Phys. Rev. E* **2000**, *61*, 2848.
(16) Matsen, M. W. *J. Chem. Phys.* **1997**, *106*, 7781.
(17) Geisinger, T.; Müller, M.; Binder, K. *J. Chem. Phys.* **1999**, *111*, 5241.
(18) Fredrikson, G. *Macromolecules* **1987**, *20*, 2535.
(19) Tsori, Y.; Andelman, D. *Europhys. Lett.* **2001**, *53*, 722.
(20) Tsori, Y.; Andelman, D. *Eur. Phys. J. E* **2001**, *5*, 605.
(21) Tsori, Y.; Andelman, D. *Macromolecules* **2005**, *38*, 7193.

(22) Tsori, Y.; Andelman, D. *Macromolecules* **2003**, *36*, 8560.

(23) Khandpur, A. K.; Foerster, S.; Bates, F. S.; Hamley, I. W.; Ryan, A. J.; Bras, W.; Almdal, K.; Mortensen, K. *Macromolecules* **1995**, *28*, 8796.

(24) Gido, S. P.; Gunther, J.; Thomas, E. L.; Hoffman, D. *Macromoleculs* **1993**, *26*, 4506.

(25) Gido, S. P.; Thomas, E. L. *Macromolecules* **1994**, *27*, 6137.

(26) Hashimoto, T.; Koizumi, S.; Hasegawa, H. *Macromolecules* **1993**, *27*, 1562.

(27) Detcheverry, F. A.; Pike, D. Q.; Nagpal, U.; Nealey, P. F.; de Pablo, J. J. *Soft Matter* **2009**, *5*, 4858.

(28) Man, X. K.; Andelman, D.; Orland, H. *Phys. Rev. E* **2012**, *86*, 010801.

(29) Coulon, G.; Russell, T. P.; Deline, V. R. *Macromolecules* **1989**, *22*, 2581.

(30) Knoll, A.; Horvat, A.; Lyakhova, K. S.; Krausch, G.; Sevink, G. J. A.; Zvelindovsky, A. V.; Magerle, R. *Phys. Rev. Lett.* **2002**, *89*, 035501.

(31) Knoll, A.; Magerle, R.; Krausch, G. *J. Chem. Phys.* **2004**, *120*, 1105.

(32) Stoykovich, M.; Müller, M.; Kim, S.; Solak, H.; Edwards, E.; de Pablo, J. J.; Nealey, P. F. *Science* **2005**, *308*, 1442.

(33) Ruiz, R.; Kang, H. M.; Detcheverry, F. A.; Dobisz, E.; Kercher, D. S.; Albrecht, T. R.; de Pablo, J. J.; Nealey, P. F. *Science* **2008**, *321*, 936.

(34) Bang, J.; Jeong, U.; Ryu, D. Y.; Russell, T. P.; Hawker, C. J. *Adv. Mater.* **2009**, *21*, 4769.

(35) Segalman, R.; Yokoyama, H.; Kramer, E. J. *Adv. Mater.* **2001**, *13*, 1152.

(36) Stein, G. E.; Lee, W. B.; Fredrickson, G. H.; Kramer, E. J.; Li, X.; Wang, J. *Macromolecules* **2007**, *40*, 5791.

(37) Li, H.-W.; Huck, W. T. S. *Nano Lett.* **2004**, *4*, 1633.

(38) Voet, V.; Pick, T.; Park, S.-M.; Moritz, M.; Hammack, A.; Urban, D.; Ogletree, D.; Olynick, D.; Helm, B. *J. Am. Chem. Soc.* **2011**, *133*, 2812.

(39) Thebault, P.; Niedermayer, S.; Landis, S.; Chaix, N.; Guenoun, P.; Daillant, J.; Man, X. K.; Andelman, D.; Orland, H. *Adv. Mater.* **2012**, *24*, 1952.

(40) Rubinstein, M.; Colby, R. H.; *Polymer Physics*; Oxford University: New York, 2003.

(41) Doi, M. *Introduction to Polymer Physics*; Oxford University: Oxford, U.K., 1996.

(42) Safran, S. *Statistical Thermodynamics of Surfaces, Interfaces, and Membranes*; Westview Press: Boulder, CO, 2003.

(43) Garel, T.; Doniach, S. *Phys. Rev. B* **1982**, *26*, 325.

(44) Ohta, T.; Kawasaki, K. *Macromolecules* **1986**, *19*, 2621.

(45) Villain-Guillot, S.; Andelman, D. *Eur. Phys. J. B* **1998**, *4*, 95.

(46) Villian-Guillot, S.; Netz, R. R.; Andelman, D.; Schick, M. *Physica A* **1998**, *249*, 284.

(47) Helfand, E.; Tagami, Y. *J. Chem. Phys.* **1971**, *56*, 3592.

(48) Naugthon, J. R.; Matsen, M. W. *Macromolecules* **2002**, *35*, 5688.

(49) Note that if we include the asymmetric $v_{\phi\rho}$ term in eq 5, this will add a first harmonic term in the expansion of $\eta(x)$ of the form: $\eta_q \cos(q_0 x)$ with $\eta_q = 2v_{\phi\rho}\phi_q/(4Kq_0^2 + \varepsilon)$

(50) Burgaz, E.; Gido, S. P. *Macromolecules* **2000**, *33*, 8739.

(51) Stasiak, P.; McGraw, J. D.; Dalnoki-Veress, K.; Matsen, M. W. *Macromolecules* **2012**, *45*, 9531.

(52) Koizumi, S.; Hasegawa, H.; Hashimoto, T. *Macromolecules* **1994**, *27*, 6532.

(53) Jang, S. G.; Audus, D. J.; Klinger, D.; Krogstad, D. V.; Kim, B. J.; Cameron, A.; Kim, S.-W.; Delaney, K. T.; Hur, S.-M.; Killops, K. L.; Fredrickson, G. H.; Kramer, E. J.; Hawker, C. J. *J. Am. Chem. Soc.* **2013**, *135*, 6649.

(54) Hashimoto, T.; Sakamoto, N.; Koga, T. *Phys. Rev. E.* **1996**, *54*, 5832.

(55) Wickham, R. A.; Shi, A.-C.; Wang, Z. G. *J. Chem. Phys.* **2003**, *118*, 10293.

(56) Press, W. H.; Teukolsky, S. A.; Vetterling, W. T.; Flannery, B. P. *Numerical Recipes*; Cambridge University: New York, 1992.